HHS Public Access

Author manuscript

Anal Chem. Author manuscript; available in PMC 2015 August 11.

Published in final edited form as:

Anal Chem. 2012 January 3; 84(1): 356–364. doi:10.1021/ac202697d.

Optical Sensing by Transforming Chromophoric Silver Clusters in DNA Nanoreactors

Jeffrey T. Petty, **Sandra P. Story**, **Selina Juarez**, **Samuel S. Votto**, **Austin G. Herbst**, **Natalya N. Degtyareva**, and **Bidisha Sengupta**

Department of Chemistry, Furman University, Greenville, SC 29163

Jeffrey T. Petty: jeff.petty@furman.edu

Abstract

Bifunctional DNA oligonucleotides serve as templates for chromophoric silver clusters and as recognition sites for target DNA strands, and communication between these two components is the basis of an oligonucleotide sensor. Few-atom silver clusters exhibit distinct electronic spectra spanning the visible and near-infrared region, and they are selectively synthesized by varying the base sequence of the DNA template. In these studies, a 16-base cluster template is adjoined with a 12-base sequence complementary to the target analyte, and hybridization induces structural changes in the composite sensor that direct the conversion between two spectrally and stoichiometrically distinct clusters. Without its complement, the sensor strand selectively harbors ~7 silver atoms that absorb at 400 nm and that fold the DNA host. Upon association of the target with its recognition site, the sensor strand opens to expose the cluster template that has the binding site for ~11 silver atoms, and absorption at 720 nm with relatively strong emission develops in lieu of the violet absorption. Variations in the length and composition of the recognition site and the cluster template indicate that these types of dual component sensors provide a general platform for near infrared-based detection of oligonucleotides in challenging biological environments.

Keywords

Fluorescent Silver Clusters; DNA Templates; Biosensor

Introduction

Nanomaterials have electronic properties that are exquisitely responsive to changes in size and shape.[1] One avenue for directing both their overall dimensions and associated size distribution is inspired by biomineralization, whereby biological macromolecules guide the crystallization of skeletal components.[2] Biopolymers encode a spatial map of functional groups that both form and select specific types of nanomaterials, and nucleic acids are such a platform.[3,4] For noble metals, a general mechanistic approach is founded on the reduction

Correspondence to: Jeffrey T. Petty, jeff.petty@furman.edu.

SUPPORTING INFORMATION PARAGRAPH Supplemental figures describe the selective synthesis of a violet-absorbing cluster conjugate, the cluster environment transformed through hybridization, and alternate sensors and equivalent binding sites. This material is available free of charge via the Internet at http://pubs.acs.org.

of precursor cation complexes, in which phosphate coordination can be preempted by complexation with the heteroatomic nucleobases, and the favored binding sites depend on the solvent accessibility, the degree of protonation, and the electron distribution of the nucleobase. [5–7] An advantage of DNA is integration of base-dependent synthesis and base-pair directed assembly to yield structurally and spectroscopically-tunable aggregates.[8,9] Another distinctive feature of DNA templates is the formation of nanoparticles with chirality, imprinted through agglomeration that is dimensionally restricted.[10] Using evolutionary approaches, novel secondary structures of nucleic acids are formed to selectively associate with particular shapes and sizes of nanoparticles.[11,12]

By stringently attenuating nanoparticle growth through nucleobase coordination, silver clusters comprised of a few atoms form with short oligonucleotides.[13–16] These aqueous-stable clusters are distinguished by their sparse density of electronic states that are strongly coupled, as evident by their efficient excitation to (~10^5 M^{-1} cm^{-1}) and relaxation from (φ_f ~10–60%) excited states.[16,17] Furthermore, low energy excitation effectively couples dark trap states to the emissive manifold to recover emission signals from high background environments.[18,19] DNA templates typically host a mosaic of silver clusters, as evident by multiple electronic transitions that evolve with time and by the chromatographic resolution of mixtures of species, and this diversity can be constrained by varying the primary sequence of the DNA strand. [16,17,19,20] Our studies focus on hybridization-induced structural changes that guide silver cluster formation, and the host strand has two general components: the 5′ segment is a template for cluster with near-infrared absorption and emission while the 3′ portion recognizes a target oligonucleotide through complementary base pairing (Fig. 1A). Without this target, this bifunctional oligonucleotide is folded by a cluster with an absorption maximum of 400 nm. Accompanying target association with its 3′ site, the sensor unfolds to reveal the binding site for a relatively highly-emissive species with near-infrared absorption at 720 nm. By integrating binding sites for nanomaterials and recognition sites for target oligonucleotides, new approaches for analyte detection are being considered.[9,21–24] Our studies follow the process of silver cluster transformation between spectroscopically distinct species, which is orchestrated by structural changes in the composite sensor strand.

Experimental Methods

Oligonucleotides (Integrated DNA Technologies) were purified by desalting and dissolved in deionized water, and their concentrations were determined by absorbance using molar absorptivities based on the nearest-neighbor approximation. The synthetic procedure follows two general steps. First, clusters are formed on the sensor strand by combining the oligonucleotide and Ag^+ at a 1:4 relative ratio, respectively, with an oligonucleotide concentration of 90 μM in the following buffers:. citric acid/citrate (Acros) at pH = 6.8, cacodylic acid/cacodylate (Ted Pella) at pH = 7.7, or boric acid/borate (Fisher) at pH = 8.0. In these buffers, the components have net concentrations of 10 mM. An aqueous solution of BH_4^- is added to give a final concentration of 2 BH_4^-:oligonucleotide, and the resulting solution is vigorously shaken for 1 min. A high pressure reactor (Parr) controls the oxygen/nitrogen atmosphere, and samples are exposed overnight at 100 psi. With oxygen, these conditions promote absorption at 400 nm. Second, the resulting cluster-laden sensor strand

is diluted in a buffer to a typical concentration of 30 μM, and the complement to the 3′ segment of the sensor is added. After heating for 5 min, samples equilibrate at room temperature prior to spectral, chromatographic, and elemental analysis.

Absorption spectra were acquired on a Cary 50 (Varian), and emission spectra were acquired on a Fluoromax-3 (Jobin Yvon Horiba). Fluorescence correlation spectroscopy studies were conducted using diode laser excitation at 690 nm with current and temperature control (LTC100, Thorlabs), and the emission was collected by two actively-quenched single-photon counting avalanche photodiode detectors (SPCM-AQR14, Perkin Elmer) using a Hanbury Brown-Twiss setup.[25,26] The resulting TTL signal outputs were cross correlated (Flex02-01D, Correlator.com) gave an autocorrelation free of afterpulsing artifacts. Size exclusion chromatography used a 300 × 7.8 mm i.d. column (BioSep, Phenomenex) on a HPLC system (Prominence, Shimadzu) using a 10 mM citrate buffer at pH = 7 with 40 mM $NaClO_4$ to minimize matrix adsorption.[27] Absorbance and fluorescence measurements of the separated species were made using the SPD-M20A and RF-10XL, respectively. For the thymine oligonucleotides dT_5, dT_{10}, dT_{15}, dT_{20}, and dT_{30}, the averages and standard deviations of the retention times were linearly correlated to the hydrodynamic radii, from which the radii of the cluster conjugates were determined using standard error propagation methods.[28] A minimum of five measurements were made using separately prepared samples. After HPLC purification, the quantity of silver in the resulting DNA-conjugate was determined by inductively coupled plasma-atomic emission spectroscopy (Liberty Series II, Varian). Standard solutions of silver nitrate related the emission signal at 328.068 nm to the silver concentrations. Using the same buffer containing the cluster-DNA species, samples with known relative amounts Ag^+ and $C_3AC_3AC_3TC_3ACCCGCCGCTGGA$ were used as controls. The DNA concentrations were determined by the absorbance at 260 nm using the extinction coefficients of the native oligonucleotides. As suggested by λ_{max} values that differ by 1–2 nm between the oligonucleotide alone and the cluster conjugate, the electronic transitions of the nucleobases are weakly perturbed by the bound cluster, as might be expected if the cluster interacts with a small fraction of the nucleobases in the sensor strand. Standard deviations were derived from three measurements made on three separately-prepared samples of cluster-DNA conjugates.

Results

These studies were motivated by Figures 1A/B: hybridization of the short target strand 5′-TCCAGCGGCGGG-3′ with the sensor $C_3AC_3AC_3TC_3A$-CCCGCCGCTGGA tempers absorption at 400 nm in lieu of a new electronic transition at 720 nm having strong emission (see $T\text{-}S_A + S_{Ac}$ in Table 1). This coordinated response depends on both components in the sensor: a 3′ recognition site affixed to a 5′ cluster template. Severing their covalent linkage yields a diversity of species, with prominent absorption in the near-infrared that has been previously observed for the isolated $C_3AC_3AC_3TC_3A$ cluster template (Fig. 1C).[19] In contrast, the composite sensor adopts a binding site that stabilizes a single type of cluster with 400 nm absorption. *Our studies focus on restoration of the single near-infrared cluster binding site by modifying the secondary structure of the sensor strand using hybridization, and three issues are addressed.* First, the precursor cluster with λ_{max} = 400 nm is selectively

synthesized and forces a compact DNA conjugate. Second, base-pairing with the target opens the sensor strand, thereby transforming the cluster environment to favor a new species with λ_{max} = 720 nm. Third, sensors with alternate recognition sites and cluster templates respond similarly to hybridization, indicating common binding sites host these two types of metallic chromophores.

Selective Synthesis of a Violet-Absorbing Cluster

Using absorption spectroscopy to comprehensively evaluate the DNA-bound clusters, the distribution of sensor-bound clusters was narrowed to a species with λ_{max} = 400 nm by adjusting three general reaction parameters. First, relatively low precursor concentrations limit agglomeration and consequently the distribution of species (Fig. 2A/B and 1S-A). The sensor strand supports clusters with λ_{max} = 400, 435, and 535 nm, and these transitions evolve over time and respond to the relative amounts of Ag^+ and BH_4^-. In this work, 4 Ag^+ and 2 BH_4^-:oligonucleotide were used, and the corresponding silver loading of 1 Ag^+:7 bases is consistent with the formation of low-stoichiometry clusters. Second, higher oxygen concentrations accelerate the time-dependent spectral changes (Fig. 2B). Earlier studies of thymine oligonucleotides demonstrated that oxic and anoxic conditions influence the types of clusters, and similar results are obtained with the $C_3AC_3AC_3TC_3A$-based sensor.[29] In relation to a reference sample exposed to air, ~10 atm N_2 hinders while ~10 atm O_2 advances the spectral development. This distinction suggests that the 400 nm species is favored by oxidizing conditions, as also indicated by a similar response to hydrogen peroxide (Fig. 1S-B). These results indicate that a partially oxidized cluster forms, and prior studies have established the sensitivity of both silver clusters and nanoparticles to oxidation. [30,31] Third, the 400 nm cluster is exclusively formed in 10 mM buffers, while a greater diversity of species develops in buffers supplemented with 200 mM $NaClO_4$, with particularly prominent near-infrared absorptions that are also featured by $C_3AC_3AC_3XC_3Y$ (X=T/G and Y=A; X = A and Y = G) (Fig. 2C).[19,26] The similar behavior exhibited by these latter isolated cluster templates and the composite sensor strand suggests that higher salt concentrations expose binding sites on the template portion of the sensor strand. In addition to the citric acid/citrate buffer at pH 6.7, cacodylic acid/cacodylate (pH = 6.7) and boric acid/borate (pH = 8.0) buffers also support the cluster to show that its formation does not depend on the buffer components or pH (Fig. 1S-C). Following formation of the 400 nm absorbing cluster using low ionic strength, these conjugates are subsequently stable in higher ionic strength buffers, and this insensitivity is the linchpin of our hybridization-induced spectral studies.

The spectral changes triggered by the target strand emanate from the cluster-driven condensation of the sensor strand. Two observations indicate that the 400 nm absorbing species is conjugated with the sensor strand: the cluster exhibits a circular dichroism response due to its association with DNA and the chromatographically isolated species has absorptions due to both the cluster and DNA at 400 and 260 nm, respectively (Fig. 3C/D). The overall shape of this complex is smaller in relation to the oligonucleotide alone, as determined from size exclusion chromatography (Fig. 3A). Using size standards based on thymine oligonucleotides, hydrodynamic radii of 1.6 ± 0.1 nm and 1.0 ± 0.1 nm were derived for the oligonucleotide and its cluster conjugate, respectively, and the former size is

consistent with a single-stranded 28-base oligonucleotide in a random coil conformation.[32–34] Thus, the cluster reduces the oligonucleotide size by ~38%, which may be related to electrostatic interaction of the partially oxidized cluster with the polyanionic backbone of the oligonucleotide. The purity of the chromatographically-resolved species is supported by its sparse electronic spectrum, with absorptions only at 400 nm from the cluster and at 260 nm from the nucleobases. Isolation of this species and subsequent concentration measurements yielded a relative stoichiometry of 7.2 ± 1.2 Ag/oligonucleotide ($T\text{-}S_A$ in Table 1), consistent with the small sizes of chromophoric silver clusters.[19,26,35] We expect that the proximity of the DNA-bound silver atoms will promote strong electronic coupling, and we are investigating the relationship between empirical stoichiometry and cluster size by identifying cluster binding sites. The absorption spectrum of this cluster-DNA complex differs from that of similarly sized silver clusters stabilized by thiols, which may reflect how the coordinating ligands alter the electronic environment of these small clusters.[36,37]

Hybridization Transforms the Structure of Sensor and Cluster Environment

Our central observation is that adding the target to the cluster-laden sensor diminishes the absorbance at 400 nm while promoting a new band at 720 nm (Fig. 1A). In support of a hybridization-dependent process, the reaction is checked by a noncomplementary strand and is insensitive to the pH and buffer components (Fig. 2S-A and 1S-C). Target binding to the single 3′ recognition site in the sensor is confirmed through spectroscopically-derived inflections at ~1 target:sensor at both 400 and 720 nm (Fig. 1D and 2S-B). The rate of this transition to the cluster-conjugated duplex suggests that the association reaction is inhibited, possibly due to cluster-dictated folding in the sensor. This hindrance is alleviated by higher concentrations of $NaClO_4$ and by polycationic amines, indicating that backbone neutralization promotes duplex stability and thus opening of the sensor strand (Figs. 2S-C/D). Temperature also influences the transformation (Fig. 3S-A). In a buffer with 200 mM $NaClO_4$, the absorbance at 720 nm is prominent at 60 °C but is not recovered at higher temperatures, which is attributed to thermal instability of the clusters. Correlated absorbance changes at 400 and 720 nm suggest that distinct clusters are transformed through hybridization with the sensor, and this evolution is also supported by directly quantitating the formation of the near-infrared emissive clusters (Fig. 1E and F). Because of their high molecular brightness, cluster occupancy in an optically defined probe volume was measured using fluorescence correlation spectroscopy. With graded addition of the complement, the number of near-infrared emissive clusters linearly tracks the absorbance changes at 720 nm, supporting conversion of the dark 400 nm absorbing species to the emissive 720 absorbing species. The cluster evolution also occurs when the structurally-distinct, cluster-laden strand is isolated from other components in the reaction mixture using size exclusion chromatography (Fig. 3S-B), suggesting that the spectral changes are exclusively associated with the 400 nm absorbing species. In addition, the transformation depends on the concentration of the cluster-DNA conjugate, indicating that intermolecular exchange leads to cluster evolution (Fig. 3S-C).

This spectral transformation is accompanied by opening of the host strand, as evident in the weaker retention and hence larger global size of the 720 nm absorbing cluster conjugate in

relation to the 400 nm absorbing cluster analog (Fig. 3A). Without the cluster, the sensor duplex has a hydrodynamic radius of 2.1 ± 0.1 nm, which is consistent with the net hydrodynamic radius derived from separate measurements of the 12 base-pair duplex and 16 base cluster template. With the 720 nm absorbing cluster, this radius increases to 3.6 ± 0.2 nm, supporting opening of the host that exposes the binding site for the near-infrared cluster. The larger size of this cluster conjugate in relation to the oligonucleotide host indicates that this cluster alters the size of its host, as previous studies have observed for red-emitting clusters.[38] Because it could also be chromatographically resolved, the 720 nm absorbing species was isolated, and its stoichiometry was determined to be 11.0 ± 1.2 Ag:oligonucleotide (T-S_A + S_{Ac} in Table 1). Thus, the hybridized sensor hosts a cluster with a similar stoichiometry as $C_3AC_3AC_3TC_3A$ alone, suggesting that hybridization reveals this same binding site on the sensor.[19] The ~4 Ag atom stoichiometry difference between the two spectrally-resolved clusters shows that transforming the binding sites promotes further agglomeration.

Alternate Sensors and Equivalent Binding Sites

This spectral transformation is also accomplished with sensor strands that differ in the length and composition of the recognition element as well as the cluster template (Table 1 and Fig. 4S). The effect of the length and composition of the recognition sites is considered using T-S_B, T-S_C and T-S_D, in which the 3′ appendages to the $C_3AC_3AC_3TC_3A$ template are a truncated variant of S_A, a 22 base recognition element for a cancer-related microRNA, and a 19 base recognition element for the exon 6 of the human GAPDH gene, respectively.[39,40] In relation to $C_3AC_3AC_3TC_3A$-CCCGCCGCTGGA (T-S_A in Table 1) discussed above, the polarity of the recognition element is reversed in T-S_E, and the cluster template is modified by replacing guanine for thymine in G-S_E.[26] Similar spectra with λ_{max} ~ 400 nm are exhibited by all the sensor strands, with variations in the efficiency of cluster formation and in the electronic environment reflected in the absorbances and λ_{max} values, respectively. While absorption at 400 nm dominates all the spectra, some sensors also exhibit absorbance at 720 nm, suggesting that the environmental distinction between the two types of clusters has been influenced. Commonality extends to how these sensors respond to the appropriate complement: diminished absorbance at 400 nm countered by enhanced absorbance at 720 nm. A conversion between two common types of clusters is supported by the reaction G-S_E + S_{Ec}, as the isolated cluster template $C_3AC_3AC_3GC_3A$ hosts the same cluster as $C_3AC_3AC_3TC_3A$.[26] Two conclusions are drawn from the studies with the 6-base recognition element (T-S_B + S_{Bc}). First, formation of the 400 nm absorbing cluster with this short appendage indicates that the cluster favors the junction between the template and recognition components. Second, the spectral transformation is less complete with the shorter complement/target pair, which again indicates that cluster-induced folding impedes target binding and is more pronounced with a shorter, lower affinity target.

Discussion

When a target oligonucleotide base pairs with the 3′ recognition site of a two-component sensor strand, a violet-absorbing cluster is converted to a near infrared-absorbing counterpart, thus highlighting how DNA-bound silver clusters adapt to their strand

environment. Prior studies have demonstrated that small silver clusters are anchored by nucleobase coordination, as shown by the enhanced emission accompanying selective deprotonation of the endocyclic nitrogens, by the effect of nitrogen and/or oxygen coordination on X-ray scattering from the clusters, and by the energetic preference of silver clusters for the N3 of cytosine.[20,29,41,42] Longer-range, multi-base interactions are deduced from the sequence-encoded formation of spectrally-diverse clusters and from the base-dependence of the excited state dynamics.[16,17,19,26,43] Further perspective on the global DNA matrix is gained by pH coupling of the cluster emission and DNA folding in a conjugate that mimics an i-motif construct.[33] Two studies provide context for the central thesis of this work: the nucleobase environment for particular clusters can be redirected through base pairing. First, thorough manipulation of the strand components was used with comparative structural analysis using gel electrophoresis, and these results demonstrated that complementary oligonucleotides produce new clusters when they hybridize with the cluster-based reporter strand.[21,44] The composition and length of the reporter component determines the types and stability of the newly formed clusters. A second study considered static quenching in which base pairing blocked the favored binding sites for a near-infrared emitting species.[23] DNA-directed, in situ synthesis of new silver clusters relieved this fluorescence quenching, as determined through the direct enumeration of emissive species using fluorescence correlation spectroscopy. This is a distinguishing mechanism of fluorescence sensing, and a principal contribution from the present studies is the identification and the characterization of the original and terminal clusters in this hybridization process using spectrometry, chromatography, and stoichiometry studies. The sensor strand exclusively hosts ~7 atoms with absorption at 400 nm, but the complementary target strand converts the violet-absorbing cluster to an ~11 atom conjugate with absorption at 720 nm and relatively strong emission.

The spectral and stoichiometric changes are consistent with cluster evolution, as experimental and theoretical studies have established that small (~10 atoms) silver clusters possess diverse electronic spectra that depend on factors such as size and charge.[35,45–47] For our DNA-bound clusters, the reaction is inhibited at lower concentrations, suggesting that agglomeration occurs via intermolecular transfer (Fig. 3S-C). Two steps narrowed the range of species involved in this process. First, the reaction conditions restricted the distribution of DNA-bound clusters to produce a structurally-distinct conjugate with a single absorption band at 400 nm (Fig. 2). Second, using size exclusion chromatography, the compactness of this DNA complex allowed it to be separated from other species that might be smaller (e.g. Ag^+) and larger (e.g. sensor only). Because the mobile phase matches the conditions for hybridization and cluster transformation, this continuity of the buffer conditions helped preserve the cluster integrity by shortening the time between isolation and hybridization. The same spectral transformation is observed in the purified and unpurified samples, which suggests that the spectral transformation originates with the 400 nm absorbing species (Fig. 3S-B). The change is again attributed to the 7 to 11 atom transformation, which was derived using the silver and DNA concentrations derived from chromatographically-purified samples. Having established that hybridization induces spectroscopic, stoichiometric, and structural changes, we are now focused on a more detailed understanding of the transformation, and one avenue we are pursuing is the use of reversed-phase

chromatography to provide greater resolution of the DNA-bound clusters. Another possibility is that the hybridizing strand could bring silver to the sensor during hybridization. However, this strand is added after the clusters are synthesized and no spectral changes are observed when the complement is added in low salt buffers where hybridization is arrested (Fig. 2S-D).

Another key finding of our studies is that the binding sites are molded by their metallic ligands, and two previous studies emphasize how DNA structure is impacted by silver clusters. First, an extended cytosine-based template is devoid of proton-mediated base-pairing at high pH and adopts a random coil conformation, while complexation with a green-emitting cluster produces a conjugate resembling a compact i-motif construct.[33] Second, structural changes in the host strand also depend on the type of cluster. In relation to the single-stranded templates alone, green emitting clusters decrease the hydrodynamic radii of the host DNA by 12 – 26% while their red-emitting counterparts increase the overall size by 14%.[38] In both studies, the generality of the observations is buttressed by using different DNA templates to host the same silver cluster. In the present studies, the sensor exclusively harbors a violet-absorbing cluster that folds the DNA strand in relation to its inherent random coil conformation. Severing the cluster template and the recognition site destroys the environment for this cluster, indicating the longer oligonucleotide folds to specify the appropriate environment. Because the cluster is favored under oxidizing conditions, partial oxidation may alleviate electrostatic repulsion between the phosphates, thereby promoting condensation. The thermodynamic impact of the ~38% reduction of the hydrodynamic radius is reflected in the inhibited target association, which is circumvented with higher ionic strength buffers and longer recognition sites. The fundamental finding of our work is that this folding precludes formation of the near-infrared absorbing species, but the DNA binding site is recovered through hybridization with the target strand.

In one respect, these cluster-based sensors are analogous to molecular beacons: secondary structural changes in the sensor strand accompany analyte binding to give a spectral response.[48,49] In molecular beacons, the spectral change is based on distance-dependent, electronic coupling of chromophores. In contrast, secondary structural changes in the cluster-laden sensor open new binding sites for DNA-directed, in situ cluster synthesis, and the conversion is accompanied by a substantial spectral shift because of the strong dependence of the electronic spectra on stoichiometry and oxidation state. This conversion to an optically and stoichiometrically distinct cluster is now being considered as an alternative approach to sensing analytes in biological environments. From 650 – 900 nm, a low spectral background in conjunction with the high molecular brightness of the near-infrared fluorophore favors sensitive analysis in spectrally-challenging blood and serum samples.[50–52] Thus, this approach may facilitate oligonucleotide analysis by reducing sample preparation. We are also considering if other spectrally distinct chromophores can be similarly prepared, with the goal of multiplexed analysis.[44]

Conclusion

Diverse functionality from DNA can be harnessed using its predictable base pairing relationships, and this utility is enhanced by also using the nucleobases as binding sites for

nanomaterials. Our studies follow the evolution of DNA bound silver clusters as the structure of a bifunctional sensor strand responds to hybridization with a complementary target strand. With a more thorough understanding of cluster transformation using DNA templates, the development of sensors for challenging biological environments will be facilitated.

Supplementary Material

Refer to Web version on PubMed Central for supplementary material.

Acknowledgments

We thank the National Science Foundation (CBET-0853692) for support of this work. We are grateful to the National Institutes of Health (R15GM071370) for primary support during the initial stages of this work. In addition, we thank the National Science Foundation (CHE-0718588 and CHE-0922834), Henry Dreyfus Teacher-Scholar Awards Program, and the National Institutes of Health (P20 RR-016461 from the National Center for Research Resource) for their support throughout this project. We are also grateful the Furman Advantage program for their commitment to student support.

References

1. Burda C, Chen X, Narayanan R, El-Sayed MA. Chem Rev. 2005; 105:1025–1102. [PubMed: 15826010]
2. Weiner S, Sagi I, Addadi L. Science. 2005; 309:1027–1028. [PubMed: 16099970]
3. Coppage R, Slocik JM, Briggs BD, Frenkel AI, Heinz H, Naik RR, Knecht MR. J Am Chem Soc. 2011; 133:12346–12349. [PubMed: 21774561]
4. Berti L, Burley GA. Nat Nanotechnol. 2008; 3:81–87. [PubMed: 18654466]
5. Lippert B. Coord Chem Rev. 2000; 200–202:487–516.
6. Sivakova S, Rowan SJ. Chem Soc Rev. 2005; 34:9–21. [PubMed: 15643486]
7. Clever G, Reitmeier S, Carell T, Schiemann O. Angew Chem Int Ed. 2010; 49:4927–4929.
8. Carter JD, LaBean TH. ACS Nano. 2011; 5:2200–2205. [PubMed: 21314176]
9. Tikhomirov G, Hoogland S, Lee PE, Fischer A, Sargent EH, Kelley SO. Nat Nanotechnol. 2011; 6:485–490. [PubMed: 21743454]
10. Shemer G, Krichevski O, Markovich G, Molotsky T, Lubitz I, Kotlyar AB. J Am Chem Soc. 2006; 128:11006–11007. [PubMed: 16925401]
11. Gugliotti LA, Feldheim DL, Eaton BE. Science. 2004; 304:850–852. [PubMed: 15087507]
12. Franzen S, Leonard DN. J Phys Chem C. 2011; 115:9335–9343.
13. Petty JT, Zheng J, Hud NV, Dickson RM. J Am Chem Soc. 2004; 126:5207–5212. [PubMed: 15099104]
14. Gwinn EG, O'Neill P, Guerrero AJ, Bouwmeester D, Fygenson DK. Adv Mater. 2008; 20:279–283.
15. Schultz D, Gwinn E. Chem Commun. 2011
16. Sharma J, Yeh HC, Yoo H, Werner JH, Martinez JS. Chem Commun. 2010; 46:3280–3282.
17. Richards CI, Choi S, Hsiang JC, Antoku Y, Vosch T, Bongiorno A, Tzeng YL, Dickson RM. J Am Chem Soc. 2008; 130:5038–5039. [PubMed: 18345630]
18. Richards CI, Hsiang JC, Senapati D, Patel S, Yu J, Vosch T, Dickson RM. J Am Chem Soc. 2009; 131:4619–4621. [PubMed: 19284790]
19. Petty JT, Fan C, Story SP, Sengupta B, St John Iyer A, Prudowsky Z, Dickson RM. J Phys Chem Lett. 2010; 1:2524–2529. [PubMed: 21116486]
20. Ritchie CM, Johnsen KR, Kiser JR, Antoku Y, Dickson RM, Petty JT. J Phys Chem C. 2007; 111:175–181.

21. Yeh HC, Sharma J, Han JJ, Martinez JS, Werner JH. Nano Lett. 2010; 10:3106–3110. [PubMed: 20698624]
22. Lan GY, Chen WY, Chang HT. Biosensors and Bioelectronics. 2011; 26:2431–2435. [PubMed: 21074985]
23. Petty JT, Sengupta B, Story SP, Degtyareva NN. Anal Chem. 2011; 83:5957–5964. [PubMed: 21702495]
24. Yang SW, Vosch T. Anal Chem. 2011; 83:6935–6939. [PubMed: 21859161]
25. Vosch T, Antoku Y, Hsiang JC, Richards CI, Gonzalez JI, Dickson RM. Proc Natl Acad Sci U S A. 2007; 104:12616–12621. [PubMed: 17519337]
26. Petty JT, Fan C, Story SP, Sengupta B, Sartin M, Hsiang JC, Perry JW, Dickson RM. J Phys Chem B. 2011; 115:7996–8003. [PubMed: 21568292]
27. Phan AT, Gueron M, Leroy JL. Methods Enzymol. 2001; 338:341–371. [PubMed: 11460557]
28. Bevington, P.; Robinson, DK. Data Reduction and Error Analysis for the Physical Sciences. McGraw-Hill; 2002.
29. Sengupta B, Ritchie CM, Buckman JG, Johnsen KR, Goodwin PM, Petty JT. J Phys Chem C. 2008; 112:18776–18782.
30. Henglein A, Mulvaney P, Linnert T. Faraday Discuss. 1991:31–44.
31. Cathcart N, Mistry P, Makra C, Pietrobon B, Coombs N, Jelokhani-Niaraki M, Kitaev V. Langmuir. 2009; 25:5840–5846. [PubMed: 19358597]
32. Doose S, Barsch H, Sauer M. Biophys J. 2007; 93:1224–1234. [PubMed: 17513377]
33. Sengupta B, Springer K, Buckman JG, Story SP, Abe OH, Hasan ZW, Prudowsky ZD, Rudisill SE, Degtyareva NN, Petty JT. J Phys Chem C. 2009; 113:19518–19524.
34. van Holde, KE.; Johnson, WC.; Ho, PS. Principles of Physical Biochemistry. Pearson/Prentice Hall; Upper Saddle River, NJ: 2006.
35. Bonacic-Koutecky V, Veyret V, Mitric R. J Chem Phys. 2001; 115:10450–10460.
36. Wu Z, Lanni E, Chen W, Bier ME, Ly D, Jin R. J Am Chem Soc. 2009; 131:16672–16674. [PubMed: 19886625]
37. Udaya Bhaskara Rao T, Pradeep T. Angew Chem Int Ed. 2010; 49:3925–3929.
38. Driehorst T, O'Neill P, Goodwin PM, Pennathur S, Fygenson DK. Langmuir. 2011; 27:8923–8933. [PubMed: 21682258]
39. Li J, Schachermeyer S, Wang Y, Yin Y, Zhong W. Anal Chem. 2009; 81:9723–9729. [PubMed: 19831385]
40. Tsourkas A, Behlke MA, Bao G. Nucleic Acids Res. 2002; 30:4208–4215. [PubMed: 12364599]
41. Neidig ML, Sharma J, Yeh HC, Martinez JS, Conradson SD, Shreve AP. J Am Chem Soc. 2011; 133:11837–11839. [PubMed: 21770404]
42. Soto-Verdugo V, Metiu H, Gwinn E. J Chem Phys. 2010; 132:195102. [PubMed: 20499990]
43. Patel SA, Cozzuol M, Hales JM, Richards CI, Sartin M, Hsiang JC, Vosch T, Perry JW, Dickson RM. J Phys Chem C. 2009; 113:20264–20270.
44. Hsin-Chih Y, Sharma J, Han JJ, Martinez JS, Werner JH. Nanotechnology Magazine, IEEE. 2011; 5:28–33.
45. Fedrigo S, Harbich W, Buttet J. J Chem Phys. 1993; 99:5712–5717.
46. Felix C, Sieber C, Harbich W, Buttet J, Rabin I, Schulze W, Ertl G. Chem Phys Lett. 1999; 313:105–109.
47. Félix C, Sieber C, Harbich WJB, Rabin I, Schulze W, Ertl G. Phys Rev Lett. 2001; 86:2992–2995. [PubMed: 11290090]
48. Kostrikis LG, Tyagi S, Mhlanga MM, Ho DD, Kramer RF. Science. 1998; 279:1228–1229. [PubMed: 9508692]
49. Wang K, Tang Z, Yang CJ, Kim Y, Fang X, Li W, Wu Y, Medley CD, Cao Z, Li J, Colon P, Lin H, Tan W. Angew Chem, Int Ed. 2009; 48:856–870.
50. Chance B. Ann N Y Acad Sci. 1998; 838:29–45. [PubMed: 9511793]
51. Frangioni JV. Curr Opin Chem Biol. 2003; 7:626–634. [PubMed: 14580568]
52. Campbell RE, Chang CJ. Curr Opin Chem Biol. 2010; 14:1–2. [PubMed: 20022288]

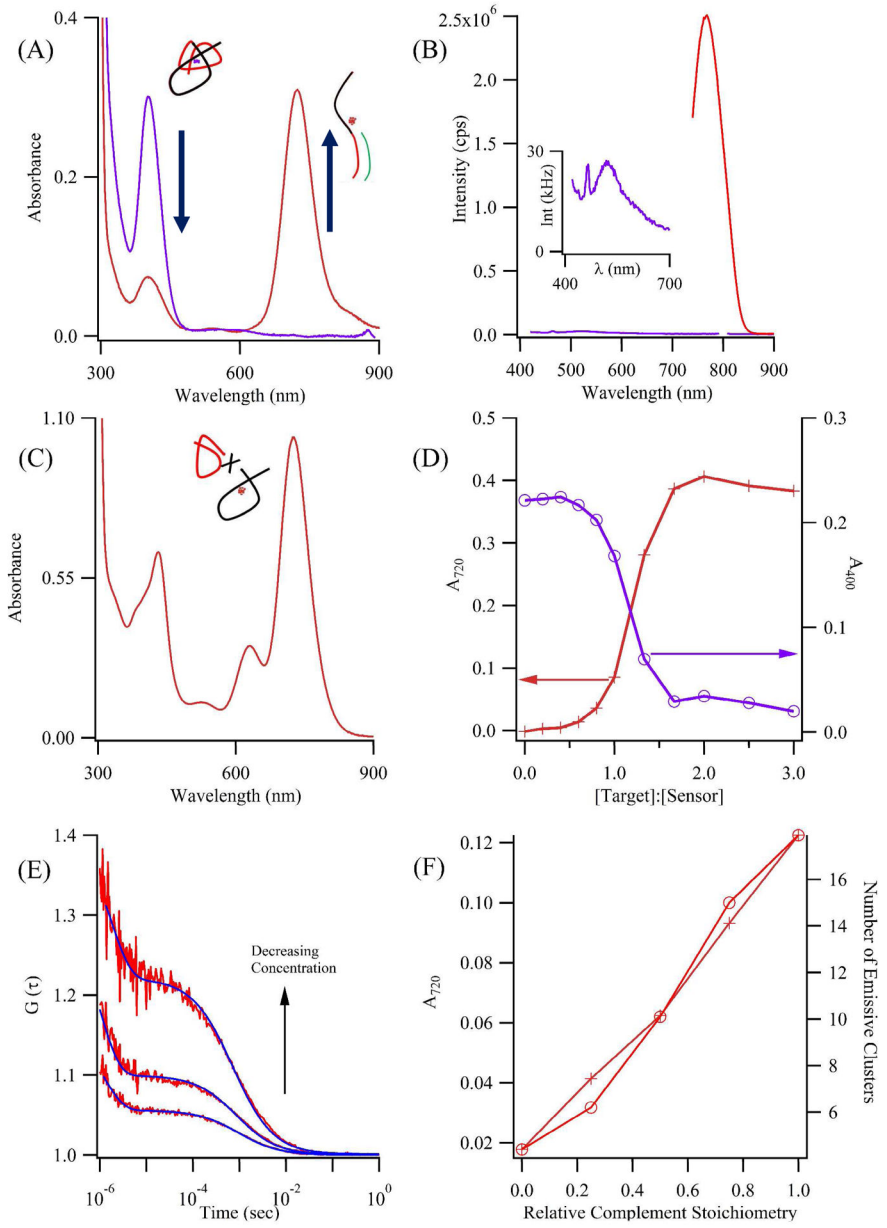

Figure 1. Hybridization Transforms the Cluster Environment

(A) and (B)-Absorption and emission spectra, respectively, of the sensor strand alone (violet) and hybridized with the 3′ complementary target strand (dark red) exhibit correlated spectral responses that support conversion of the 400 nm to the 720 nm absorbing cluster. The inset in (B) highlights the relatively weak emission using λ_{ex} = 400 nm prior to adding the complement to the sensor. (C)-Severing the cluster template and the recognition element yields prominent absorption at 720 nm. This contrast with the sole absorption at 400 nm for the composite strand (A – violet spectrum) indicates that folding by the larger oligonucleotide determines the binding site for the violet absorbing cluster. (D)-Variations in the absorbance response at 720 nm (left axis, dark red) and 400 nm (right axis, violet) with relative stoichiometry changes in the target concentration show inflection points at ~1

target:sensor (also see Fig. 2S-B), thus supporting complementary base pairing between the target and the single recognition site on the sensor. (E) and (F)-Fluorescence correlation analysis (E) allows the absorbance changes (F-left axis) to be compared with the number of emissive clusters (F-right axis). To fully model the correlation function, coupling of a dark electronic state was included in the analysis.[26] The correlation contrast for the diffusive component (E) is inversely related to the number of emitters in the optical probe volume. Because the concentrations vary linearly with the absorbance, the complementary strand induces secondary structural changes that produce new emissive species.

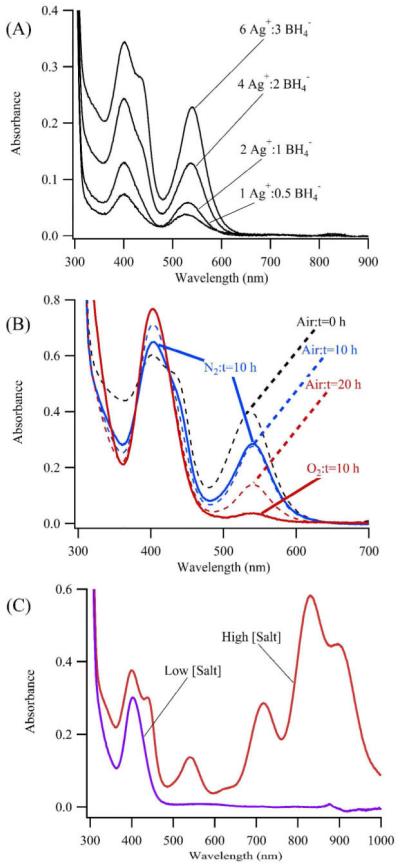

Figure 2. Selective Synthesis of a Violet-Absorbing Cluster Conjugate

Three reaction conditions were varied to optimize cluster formation. (A)-The relative amounts of Ag^+ and BH_4^- influence the distribution of species, with the absorption shoulder at 430 nm becoming less pronounced with relatively lower precursor concentrations. (B)-Oxygen favors formation of the 400 nm absorbing species, as discerned by comparing samples exposed to air, nitrogen, and oxygen. The reference sample exposed to air (dashed lines) shows a decrease in the absorbance at 540 nm and an increase in the absorbance at 400 nm over time. This progression slows with nitrogen, while the same sample exposed to oxygen shows a fuller development to favor absorption at 400 nm. (C)-Lower ionic strength buffers composed of 10 mM citric acid/citrate exclusively favor the 400 nm absorption (violet), whereas supplementing this buffer with 200 mM $NaClO_4$ produces a greater diversity of species, particularly in the near-infrared spectral region (dark red). This comparison indicates that higher salt concentrations expose alternate binding sites on the sensor strand for silver clusters.

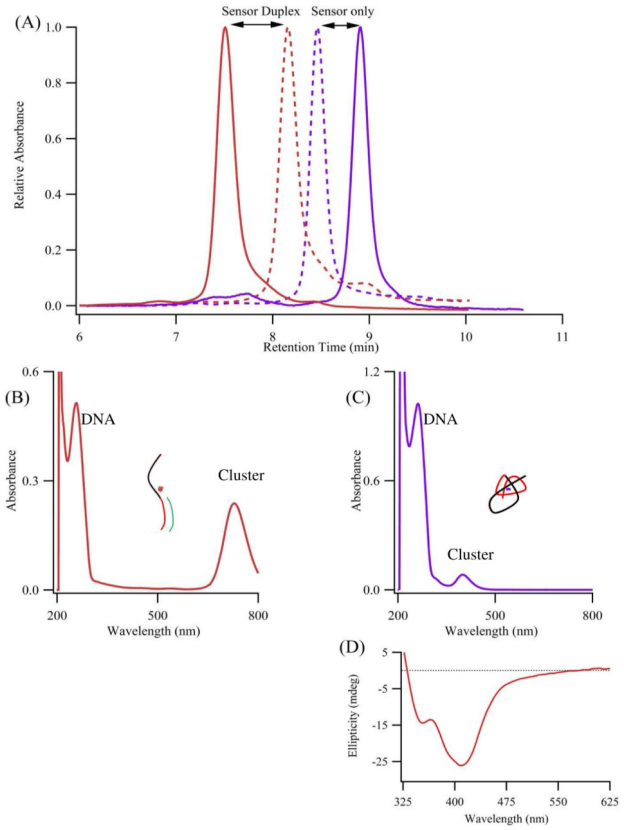

Figure 3. Hybridization Transforms the Structure of Sensor

(A)-The violet and near-infrared absorbing species are structurally distinguished by size exclusion chromatography. For the chromatograms of the single-stranded sensor without (dashed violet) and with (solid violet) the 400 nm absorbing cluster, the latter species shows absorptions only at 400 nm due to the clusters and at 260 nm due to the DNA nucleobases (C). For the duplex sensor without (dashed dark red) and with (solid dark red) the 720 nm absorbing cluster, the latter species shows absorptions only at 720 nm for the cluster and at 260 nm due to the DNA nucleobases (B). Relative absorbances are used to compare the retention times. (D)-For the single-stranded sensor, the complexed cluster exhibits a prominent response, consistent with an induced circular dichroism through association with the chiral DNA template (D).

Table 1

Oligonucleotides used for Transformation of Violet-Absorbing to Near-Infrared-Absorbing Clusters[a]

DNA Sequence	Denoted by
$C_3AC_3AC_3\underline{T}C_3A$ CCCGCCGCTGGA GGGCGGCGACCT	T-S_A + S_{Ac}
$C_3AC_3AC_3\underline{T}C_3A$ CCCGCC GGGCGG	T-S_B + S_{Bc}
$C_3AC_3AC_3\underline{T}C_3A$ TCAACATCAGTCTGATAAGCTA AGTTGTAGTCAGACTATTCGAT	T-S_C + S_{Cc}
$C_3AC_3AC_3\underline{T}C_3A$ GAGTCCTTCCACGATACCA CTCAGGAAGGTGCTATGGT	T-S_D + S_{Dc}
$C_3AC_3AC_3\underline{T}C_3A$ AGGTCGCCGCCC TCCAGCGGCGGG	T-S_E + S_{Ec}
$C_3AC_3AC_3\underline{G}C_3A$ AGGTCGCCGCCC TCCAGCGGCGGG	G-S_E + S_{Ec}

[a]The first column provides the sequences, with the following color scheme: the silver cluster template has black lettering, the recognition component has red lettering, and the target sequence has green lettering. The underlined thymine and guanine represent the modifications in the cluster template that yield the same near infrared cluster. The second column provides the abbreviations for these constructs.